

of the *median* filter, which is used for preliminary processing in most of the state-of-the-art impulsive noise filters. Our first tests on synthetic and natural images demonstrated that the *peak-and-valley* filter and the *median* filter have comparable performances. The *median* filter is slightly better than the *peak-and-valley* filter at detecting/correcting noisy pixels, but on the other hand it tends to alter more true pixels. Nevertheless, even if the amount of true pixel alterations is significant (more than 63% for the *median* filter was recorded), the average change is rather small (no more than 11 were recorded). In some applications this degradation of the image, a mild smoothing, could not readily justify a heavy computational method to discriminate between noisy and true pixels, especially when dealing with video processing. The *peak-and-valley* filter demonstrated to be much faster than the *median* filter for all types of images tested.

The *peak-and-valley* filter represents an interesting replacement for the *median* filter in those more sophisticated, and consequently more performant filtering methods, in order to improve their efficiency.

REFERENCES

- [1] A. Beläid and A. Beläid, "Reconnaissance des formes: Méthodes et applications," *InterEditions*, pp. 41–80, 1992.
- [2] S. E. Umbaugh, *Computer Vision and Image Processing: A Practical Approach*. Englewood Cliffs, NJ: Prentice-Hall, 1998, pp. 151–193.
- [3] E. Trucco and A. Verri, *Introductory Techniques for 3-D Computer Vision*. Englewood Cliffs, NJ: Prentice-Hall, 1998, pp. 51–66.
- [4] I. Pitas and A. N. Venetsanopoulos, *Nonlinear Digital Filters: Principles and Applications*. Norwell, MA: Kluwer, 1990.
- [5] H. A. David, *Order Statistics*. New York: Wiley, 1981.
- [6] D. Brownrigg, "The weighted median filter," *Commun. Assoc. Comput.*, pp. 807–818, 1984.
- [7] A. Restrepo and A. C. Bovik, "Adaptive trimmed mean filters for image restoration," *IEEE Trans. Acoust., Speech, Signal Processing*, vol. 36, no. 8, pp. 1326–1337, 1988.
- [8] S. J. Ko and Y. H. Lee, "Center weighted median filters and their applications to image enhancement," *IEEE Trans. Circuits Syst.*, vol. 38, pp. 984–993, Sept. 1991.
- [9] T. Sun and Y. Neuvo, "Detail-preserving median based filters in image processing," *Pattern Recognit. Lett.*, vol. 15, pp. 341–347, 1994.
- [10] L. Garcia-Cabrera, P. L. Luque-Escamilla, J. Martinez-Aroza, A. M. Robles-Perez, and R. Roman-Roldan, "Two pixel preselection methods for median type filtering," *IEEE Proc. Visual Image Signal Processing*, vol. 145, no. 1, pp. 30–40, 1998.
- [11] Y. Xu and E. M. Lai, "Restoration of images contaminated by mixed Gaussian and impulse noise using a recursive minimum–maximum method," *IEE Proc. Vision, Image, Signal Processing*, vol. 145, no. 4, 1998.
- [12] M. Imme, "A noise peak elimination filter," *CVGIP: Graph. Models Image Process.*, vol. 53, no. 2, pp. 204–211, 1991.
- [13] M. Werman and S. Peleg, "Min–max operators in texture analysis," *IEEE Trans. Pattern Anal. Machine Intell.*, vol. PAMI-7, no. 6, pp. 730–733, 1985.
- [14] J. Serra, "Introduction to mathematical morphology," *Comput. Vis., Graph. Image Process.*, vol. 35, no. 3, pp. 283–305, 1986.
- [15] R. M. Haralick, S. R. Sternberg, and X. Zhuang, "Image analysis using mathematical morphology," *IEEE Trans. Pattern Anal. Machine Intell.*, vol. PAMI-9, pp. 532–550, Apr. 1987.

Artifact Reduction for Set Theoretic Super Resolution Image Reconstruction with Edge Adaptive Constraints and Higher-Order Interpolants

Andrew J. Patti and Yucel Altunbasak

Abstract—In this paper, we propose to improve the POCS-based super-resolution reconstruction (SRR) methods in two ways. First, the discretization of the continuous image formation model is improved to explicitly allow for higher order interpolation methods to be used. Second, the constraint sets are modified to reduce the amount of edge ringing present in the high resolution image estimate. This effectively regularizes the inversion process.

Index Terms—Image generation, image reconstruction, image resolution, image restoration, image sampling.

I. INTRODUCTION

The topic of super resolution image reconstruction (SRR) has recently received considerable attention within the research community [1]–[3]. SRR algorithms all attempt to create a single higher resolution image from a number of lower resolution images. Although there are many flavors of these algorithms, all must first assume an image formation model relating the desired higher resolution image to the lower resolution images. Second, the high resolution image model must be inverted in some way to produce the high resolution image from the observations. Depending on the generality of the image formation model, the inversion methods must be more or less sophisticated. For example [4], a simple assumption of translational motion between low resolution images yields a linear shift-invariant system that is readily inverted in the frequency domain. When more complex motion and blurring is considered [1]–[3], [5], iterative methods need to be employed. When the SRR problem is posed in set-theoretic framework [1], [6], one of the very general and powerful tools to invert the image formation system and arrive at a solution is projections onto convex sets (POCS) [6], [7]. Concentrating on the POCS-solution for the set-theoretic SRR formulation, there are two areas where improvements are made in this paper. The first is in the image formation model. Currently, the model begins as a continuous one and is discretized by assuming the continuous high-resolution image undergoes a zero-order hold interpolation. The modeling could thus be improved by using higher order interpolants during the discretization step.

The second area where improvements can be made to existing set-theoretic formulations entails adding some form of regularization to the inversion process. Regularization is often desirable because it can reduce the visibility of artifacts created during the inversion process [8]. Probabilistic SRR formulations and solutions such as maximum a posteriori (MAP) estimators provide a simple and effective way to incorporate various regularizing constraints. Schultz and Stevenson utilized a discontinuity preserving prior within the MAP estimation context, where the likelihood of edges is controlled by the Huber edge penalty function [3], [9]. Although one of the strengths of POCS is the ability to include various constraints into the inversion process, the inclusion of regularizing constraints has been

Manuscript received October 6, 1998; revised May 1, 2000. The associate editor coordinating the review of this manuscript and approving it for publication was Prof. Patrick L. Combettes.

A. J. Patti is with the Liberate Technologies, San Carlos, CA 94070 USA (apatti@liberate.com).

Y. Altunbasak is with the School of Electrical and Computer Engineering, Georgia Institute of Technology, Atlanta, GA 30332-0250 USA.

Publisher Item Identifier S 1057-7149(01)01183-6.

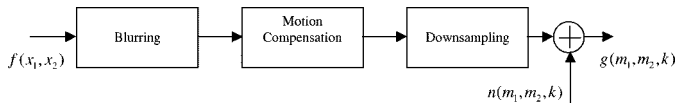


Fig. 1. Image formation model.

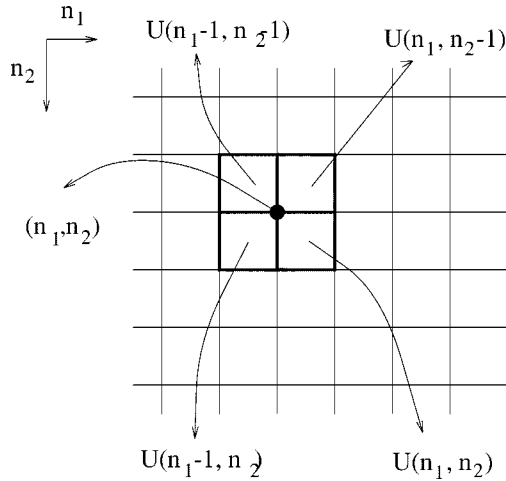


Fig. 2. High-resolution imaging plane. $U(n_1, n_2)$ denotes unit cell at the high-resolution grid point (n_1, n_2) . (m_1, m_2) refers to position of low-resolution sensor. $(m_1, m_2) \in [0, W_l - 1] \times [0, H_l - 1]$ and $(n_1, n_2) \in [0, W_h - 1] \times [0, H_h - 1]$, where W_l and H_l are the low-resolution image width and height and W_h and H_h are the high-resolution image width and height.

almost nonexistent in previous formulations, with the exception of rather trivial energy and amplitude bound constraints.

II. THEORY

We will first introduce the video image formation model with an emphasis on the discretization step in Section II-A. After discussing the commonly employed zero-order hold interpolation, we will improve the discretization stage modeling by incorporating bilinear interpolation in Section II-A2. Having understood the interplay between discretization and blurring stages in the bilinear interpolation case, we will present the inclusion of the higher order interpolants in Section II-A3. This development will yield the discrete image formation model that will be used to define the convex sets determining the high-resolution image solution. We will then delineate a regularization method used to constrain the resulting high-resolution image in Section II-B.

A. Image Formation Model

Consider the general linear shift varying (LSV) image formation model given by [1]

$$g(\boldsymbol{\ell}) = \int h_c(\boldsymbol{\ell}; \mathbf{x}) f(\mathbf{x}) d\mathbf{x}, \quad \boldsymbol{\ell} = (m_1, m_2; k), \quad \mathbf{x} = (x_1, x_2) \quad (1)$$

where $g(\boldsymbol{\ell})$ denotes the low-resolution (LR) image samples at spatial-temporal position $\boldsymbol{\ell}$ ($m_1, m_2 \in I^2$ are the low-resolution sampling lattice indices, $k \in I$ is the frame index), $f(\mathbf{x})$ is the high resolution image over the continuous domain $\mathbf{x} \in \mathbb{R}^2$, and $h_c(\boldsymbol{\ell}; \mathbf{x})$ denotes the continuous LSV blur function resulting from effects such as the optics, sensor geometry, and motion. (More specifically, $(m_1, m_2) \in [0, W_l - 1] \times [0, H_l - 1]$, $(n_1, n_2) \in [0, W_h - 1] \times [0, H_h - 1]$, $k \in [0, N]$, where W_l, H_l are the low-resolution image width and height, W_h, H_h are the high-resolution image width and height, and N is the number of

low-resolution images used to reconstruct the high-resolution image). This image formation model is depicted in Fig. 1.

It is desirable to discretize the LSV blur relationship in (1), to relate the observed LR images to a discrete version of $f(x_1, x_2)$. Thus, a discrete superposition summation of the form

$$g(\boldsymbol{\ell}) = \sum_{(n_1, n_2)} f(n_1, n_2) h_d(n_1, n_2; \boldsymbol{\ell}) \quad (2)$$

will now be formulated. We assume that the continuous imagery $f(x_1, x_2)$ is sampled on the high resolution two-dimensional (2-D) lattice Λ (i.e., (n_1, n_2) are integers that specify a point in Λ as shown in Fig. 2) to form $f(n_1, n_2)$.

1) *Discretization with Zero-order Hold:* Assuming the space of the focal plane is completely covered by some super-resolution (SR) sensor with physical dimensions that can be used as a unit cell \mathcal{U} for the lattice Λ (see Fig. 2), we can rewrite (1) as

$$g(\boldsymbol{\ell}) = \sum_{(n_1, n_2)} \int_{\mathcal{U}(n_1, n_2)} f(\mathbf{x}) h_c(\boldsymbol{\ell}; \mathbf{x}) d\mathbf{x} \quad (3)$$

where $\mathcal{U}(n_1, n_2)$ is the displaced unit cell by (n_1, n_2) . With the assumption that $f(x_1, x_2; k)$ is constant over the cell $\mathcal{U}(n_1, n_2)$, (1) can be written

$$g(\boldsymbol{\ell}) \cong \sum_{(n_1, n_2)} f(n_1, n_2) \int_{\mathcal{U}(n_1, n_2)} h_c(\boldsymbol{\ell}; \mathbf{x}) d\mathbf{x}. \quad (4)$$

By comparing (4) with (2), it is evident that

$$h_d(n_1, n_2; \boldsymbol{\ell}) = \int_{\mathcal{U}(n_1, n_2)} h_c(\boldsymbol{\ell}; \mathbf{x}) d\mathbf{x}.$$

2) *Discretization with Bilinear Interpolation:* With the zero-order hold modeling, the function $f(\mathbf{x}; k)$ is assumed constant over the high-resolution sensor $\mathcal{U}(n_1, n_2)$. However, one can better express $f(\mathbf{x}; k)$, $\mathbf{x} \in \mathcal{U}(n_1, n_2)$, in terms of $f(n_1, n_2; k)$, $f(n_1 + 1, n_2; k)$, $f(n_1, n_2 + 1; k)$, and $f(n_1 + 1, n_2 + 1; k)$ using bilinear interpolation. Specifically, approximating $f(\mathbf{x}; k)$ bilinearly, (1) can be written as

$$g(\boldsymbol{\ell}) \cong \sum_{(n_1, n_2)} \int_{\mathcal{U}(n_1, n_2)} \left[\begin{aligned} & f(n_1, n_2; k) x_1 x_2 + f(n_1 + 1, n_2; k) x_1 (1 - x_2) \\ & + f(n_1, n_2 + 1; k) (1 - x_1) x_2 \\ & + f(n_1 + 1, n_2 + 1; k) (1 - x_1) (1 - x_2) \end{aligned} \right] h_c(\boldsymbol{\ell}; \mathbf{x}) d\mathbf{x}. \quad (5)$$

Equation (5) can be rewritten as

$$g(\boldsymbol{\ell}) \cong \sum_{(n_1, n_2)} \left\{ \begin{aligned} & f(n_1, n_2; k) \int_{\mathcal{U}(n_1, n_2)} h_c(\boldsymbol{\ell}; \mathbf{x}) x_1 x_2 d\mathbf{x} \\ & + f(n_1 + 1, n_2; k) \int_{\mathcal{U}(n_1, n_2)} h_c(\boldsymbol{\ell}; \mathbf{x}) x_1 (1 - x_2) d\mathbf{x} \\ & + f(n_1, n_2 + 1; k) \int_{\mathcal{U}(n_1, n_2)} h_c(\boldsymbol{\ell}; \mathbf{x}) (1 - x_1) x_2 d\mathbf{x} \\ & + f(n_1 + 1, n_2 + 1; k) \\ & \cdot \int_{\mathcal{U}(n_1, n_2)} h_c(\boldsymbol{\ell}; \mathbf{x}) (1 - x_1) (1 - x_2) d\mathbf{x} \end{aligned} \right\}. \quad (6)$$

Noting that (n_1, n_2) is utilized four times in (6), one can reorder the terms in the summation and write

$$g(\boldsymbol{\ell}) \cong \sum_{(n_1, n_2)} f(n_1, n_2; k) h_d(n_1, n_2; \boldsymbol{\ell}) \quad (7)$$



(a)



(b)

Fig. 3. (a) Original high-resolution image and (b) one of the low-resolution images (generated from high-resolution image).

where

$$\begin{aligned}
 h_d(n_1, n_2; \ell) &= \left\{ \int_{U(n_1, n_2)} h_c(\ell; \mathbf{x}) x_1 x_2 \, d\mathbf{x} \right. \\
 &+ \int_{U(n_1, n_2)} h_c(\ell; \mathbf{x}) x_1 (1 - x_2) \, d\mathbf{x} \\
 &+ \int_{U(n_1, n_2)} h_c(\ell; \mathbf{x}) (1 - x_1) x_2 \, d\mathbf{x} \\
 &\left. + \int_{U(n_1, n_2)} h_c(\ell; \mathbf{x}) (1 - x_1) (1 - x_2) \, d\mathbf{x} \right\}. \quad (8)
 \end{aligned}$$

3) *Discretization with Higher Order Interpolants*: A more proficient approximation of the underlying continuous high-resolution image can be obtained using higher-order interpolants. To this end, we express $f(\mathbf{x})$, the continuously interpolated high-resolution image, in terms of an underlying high-resolution image $f_u(\mathbf{x})$ as

$$f(\mathbf{x}) = \left(f_u(\mathbf{x}) \sum_{\mathbf{n}} \delta(\mathbf{x} - \mathbf{n}) \right) * h_r(\mathbf{x}) \quad (9)$$

where $h_r(\mathbf{x})$ is the reconstruction interpolant, $*$ denotes two dimensional convolution, and discrete positions indexed by $\mathbf{n} = (n_1, n_2)$ are understood to be indexing the sampling lattice. Substituting (9) into (1) and carrying out straightforward manipulations yields

$$g(\ell) = \sum_{\mathbf{n}} \int f_u(\mathbf{x}) \delta(\mathbf{x} - \mathbf{n}) (h_c(\ell; \mathbf{x}) * h_r(\mathbf{x})) \, d\mathbf{x} \quad (10)$$

from which it is clear that the discretized LSV blur is

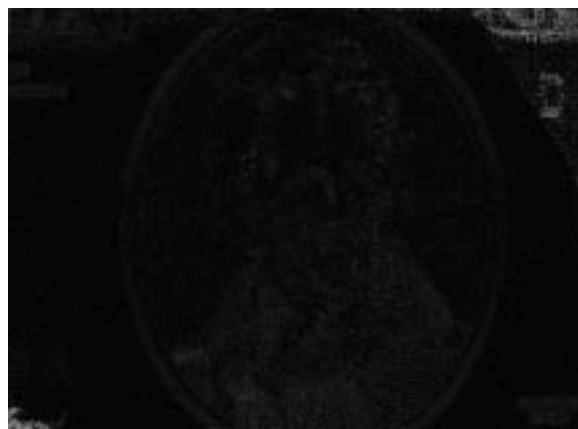
$$h_d(\mathbf{n}; \ell) = [h_c(\ell; \mathbf{x}) * h_r(\mathbf{x})]_{\mathbf{x}=\mathbf{n}}. \quad (11)$$



(a)



(b)



(c)

Fig. 4. Absolute difference images between the original and the result of SRR using (a) zero-order hold, (b) cubic, and (c) truncated sinc interpolation modeling.

TABLE I
MEAN-SQUARED-ERROR BETWEEN THE ORIGINAL AND RECONSTRUCTED IMAGE VIA POCS WITH THE DISCRETIZATION MODEL EMPLOYING a) ZERO-ORDER HOLD, b) CUBIC SPLINE, AND c) TRUNCATED SINC INTERPOLATION IS REPORTED

Discretization method	$\sigma = 0.3$	$\sigma = 1.0$	$\sigma = 5.0$
Zero-order hold	20.39	986.45	2175.82
Cubic spline interpolation	8.71	979.11	2175.80
Truncated Sinc Interpolation	3.10	955.18	2175.81

The standard POCS constraint sets are then defined based on $h_d(\mathbf{n}; \ell)$, so the inclusion of higher-order interpolants into the formulation is completely encapsulated into the blur modeling.

B. Edge Adaptive Constraints

The accuracy of blur estimation has a profound effect on the efficacy of SRR algorithms. However, in many real-life SRR applications, little information about the blur function is available. Furthermore, blur estimation techniques may produce inaccurate results. Loosely speaking, if we have a Gaussian blur with a variance σ , underestimating σ yields blurry images whereas overestimating it will cause ringing artifacts along the edges. Noting this fact, the method of adaptation for ringing suppression is to selectively modify the constraint sets defining SRR. For example, assuming that the actual blur function lies within a set of Gaussian blur functions, we could conservatively choose a blur function with a lower variance at the edge pixels, whereas in homogeneous regions, wider blur functions are selected.

To begin, the data consistency constraint sets defined based on (11) are given by

$$C(\ell) = \left\{ f(\mathbf{n}): |g(\ell) - \sum_{\mathbf{n}} f(\mathbf{n})h(\mathbf{n}; \ell)| \leq \delta_o(\ell) \right\} \quad (12)$$

where $\delta_o(\ell)$ is related to the noise in the image. The convex constraint in (12) is an l_2 norm constraint. At every low-resolution pixel a closed and convex set $C(\ell)$ is defined, and POCS SRR proceeds by successively projecting onto these sets. Unwanted ringing will be caused by projections onto sets defined at edge locations. Therefore, it is the sets defined on edges that will be modified.

A modification intended to reduce ringing must alter the sets so that projections at edges do not attempt to invert a large blur in the direction orthogonal to the edge. To reduce the amount of deblurring directly at an edge, the blur function in the direction of the edge gradient must be made more like an impulse. This is accomplished by estimating the directions of edges and then weighting the blur $h(\mathbf{n}; \ell)$ along the gradient with an appropriate function. Such a function is given below:

$$r(\mathbf{n}; \ell) = \mathfrak{R}_\theta(e^{-|\alpha^\top \mathbf{n}|}) \quad (13)$$

where θ is the edge orientation, \mathfrak{R}_θ denotes rotation operator by angle of θ , and α is selected to be proportional to the edge gradient. Although it would appear this modification would also reduce the degree of deblurring near edges, this effect is mitigated because normal projections are still carried out in the near vicinity of the edge such that the edge belongs to the support of $h(\mathbf{n}; \ell)$.

It is very important to note that by selectively changing the blur function, we may lose consistency with the observed data. In fact, the underlying physical model may be violated. Therefore, the sets may not have a common intersection. However, there are three compelling reasons to consider this method.

- 1) In practice, it provides very good results and suppresses the ringing artifacts even if the blur estimation fails.
- 2) In most applications, blur estimates are not perfect but are within some error bound. From a theoretical point of view, there is not much difference between assuming a constant erroneous blur function and selectively changing the blur function within some bound.
- 3) One may prove that for a set of functions $r(\mathbf{n}; \ell)$, the intersection of the modified sets lies within the intersection of nonmodified SRR sets. In this case, convergence is guaranteed.

III. RESULTS

Two sets of experiments are provided to demonstrate the efficacy of modeling with higher-order interpolants and edge adaptive constraints for ringing suppression. For both cases, four low-resolution images are used, and a resolution improvement by a factor of two horizontally and vertically is sought.

In the first sets of experiments, a portion of a \$20 bill is scanned at 300 dpi and used as the high-resolution image (shown in Fig. 3(a)). It is then blurred by a 9×9 gaussian filter, translated by one pixel in both horizontal and vertical directions, and decimated to obtain the low-resolution observations. The first low-resolution image is depicted in Fig. 3(b). The POCS-based SRR algorithm with 1) zero-order hold interpolation, 2) cubic interpolation, and 3) sinc interpolation [10] in the discretization stage is employed to reconstruct the original high-resolution image. Note that since a 9×9 window is also utilized in the POCS solution, sinc interpolation corresponds to a truncated sinc interpolation. Also, since no noise has been added to the LR images for this first set of experiments, δ_o is taken to be $\ll 1$. The absolute difference image between the reconstructed and original high-resolution image is shown in Fig. 4(a)–(c), respectively.

The MSE between the original and a reconstructed high-resolution image is defined as

$$\text{MSE} = \frac{1}{N} \sum_{(n_1, n_2)} (f(n_1, n_2) - \hat{f}(n_1, n_2))^2 \quad (14)$$

where $\hat{f}(n_1, n_2)$ is the reconstructed image and N is the number of pixels; and is reported for all cases in Table I. Note that the inclusion of higher-order interpolants matters most when the blur function variance is small, i.e., the smaller the blur function variance, the more important it is to account for higher order interpolants. This is expected since convolving a wide blur function with the interpolant makes a small difference (in the blur function) whereas convolving a narrow blur function with the interpolant can change its spread noticeably.

In the second sets of experiments, all low-resolution images (observations) are captured via a scanner. Motion is mostly translational but since some rotation is present an affine model is estimated. In addition, the blurring is modeled as Gaussian, while noise is present in the LR images due to the scanning operation. The value of δ_o applied to all LR observations is determined by estimating the noise variance in a smooth area of a LR image.

For the higher-order interpolant experiment the original high-resolution image is depicted in Fig. 5(a). Fig. 5(b)–(d) shows the result of SRR using, respectively, zero-order hold, cubic interpolation, and truncated sinc interpolation modeling. The cubic spline interpolation model more faithfully reproduces the original.

For the “edge adaptive constraints” experiment, Fig. 6(a) depicts the result of standard SRR with a blur assumed to be Gaussian with a standard deviation of $\sigma = 1.5$, while Fig. 6(b) shows the result of SRR with the regularization method and the same parameters/images. Fig. 7(a) and (b) show the same images for the case of blur assumed Gaussian with a standard deviation of $\sigma = 1.8$. A Sobel edge detector is utilized to locate the edge pixels [11]. We have also tested the efficiency of the proposed method with images that contain diagonal edges in addition to horizontal/vertical edges. Fig. 8(a) depicts the result of standard SRR with a blur assumed to be Gaussian with a standard deviation of $\sigma = 1.3$, while Fig. 8(b) shows the result of SRR with the regularization method.

We see that edge ringing is greatly reduced using the proposed regularization at little or no cost in terms of image sharpness. Lastly, we noticed no noticeable increase in the number of iterations required to estimate the SR image.

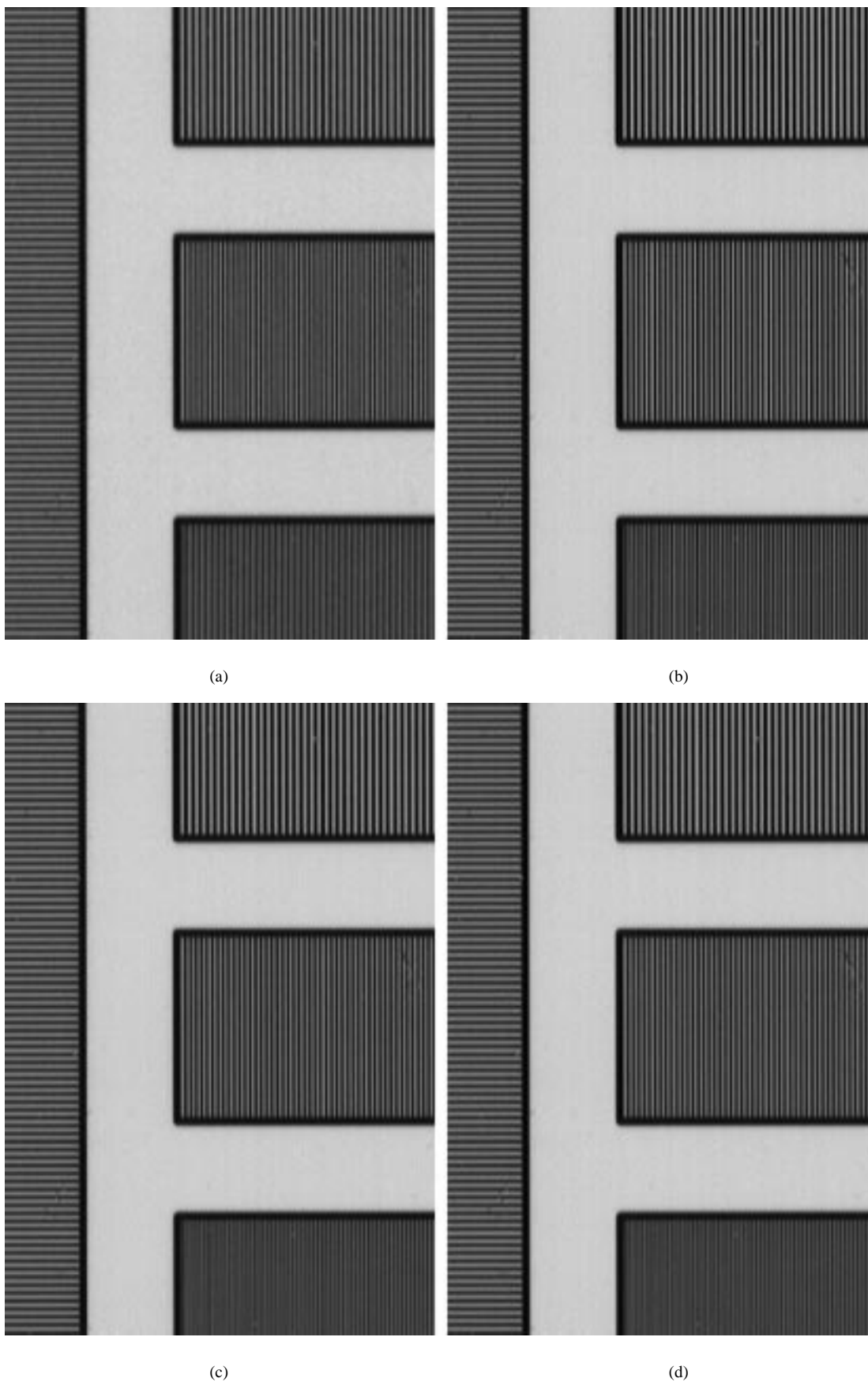
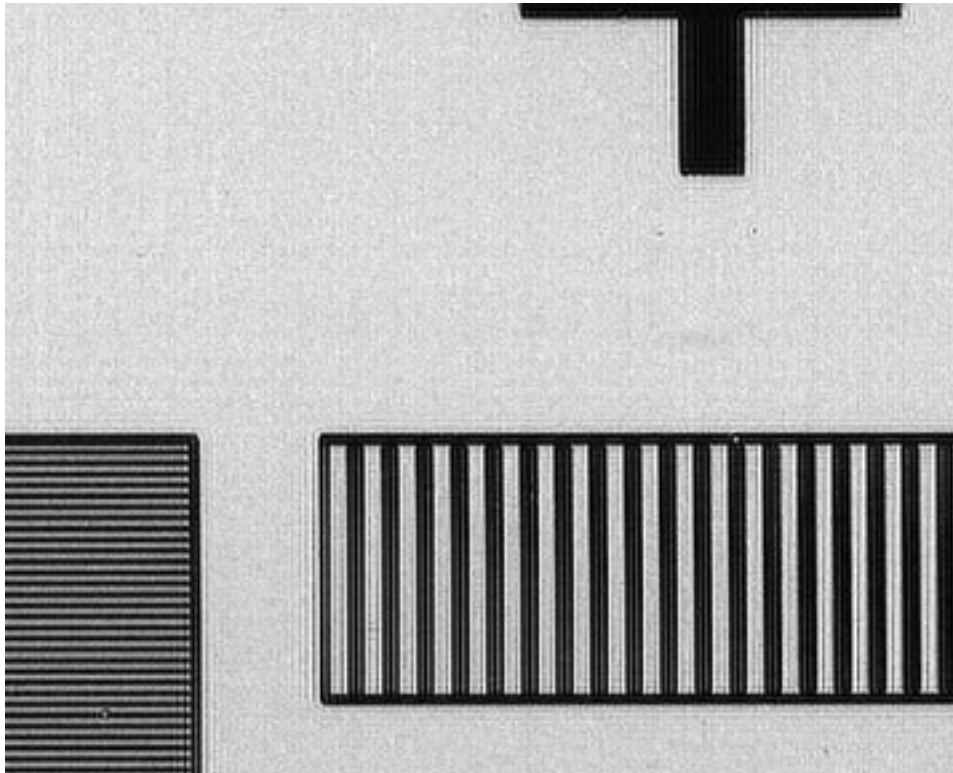
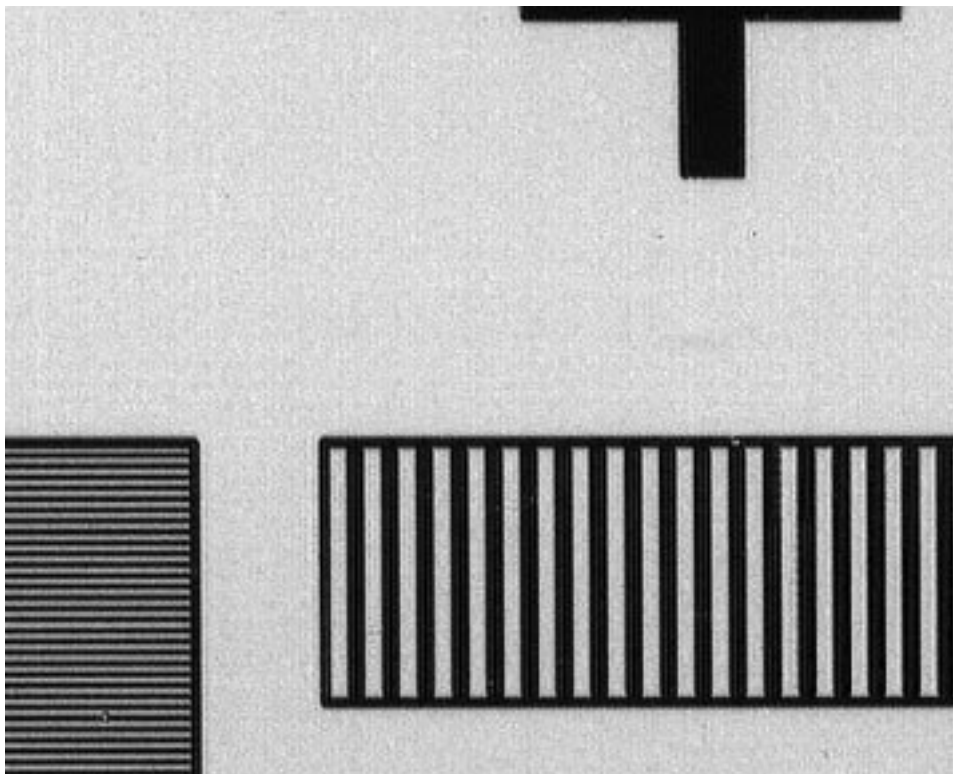


Fig. 5. (a) High-resolution image using simple bilinear interpolation to a single low-resolution image and the results of standard SRR using (b) zero-order hold, (c) cubic, and (d) truncated sinc interpolation modeling.

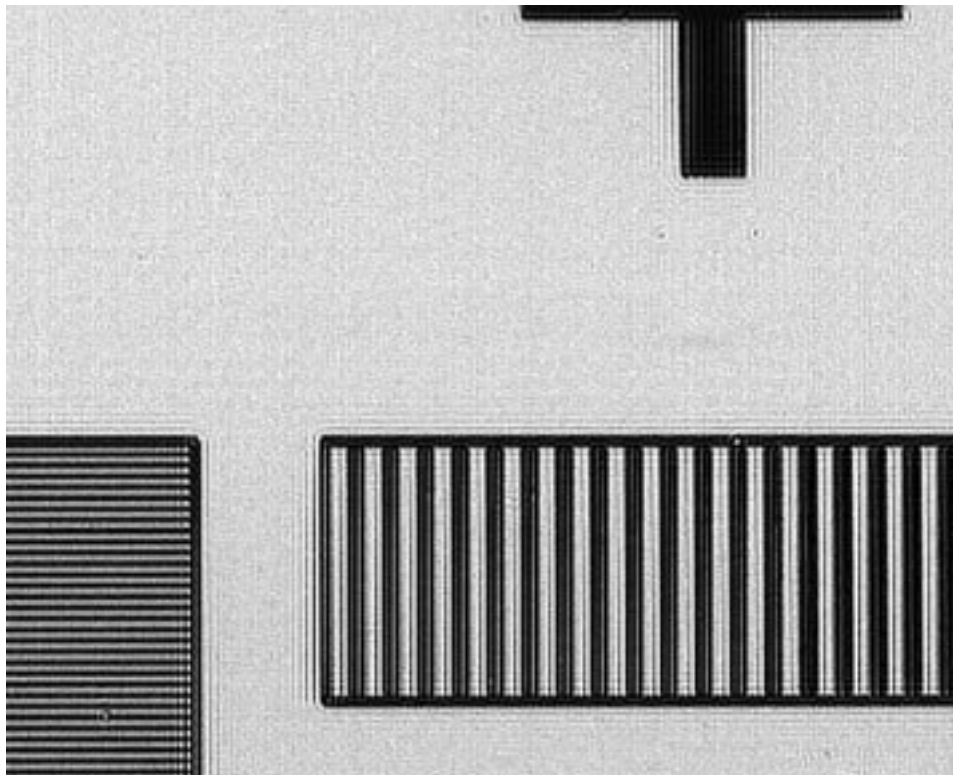


(a)

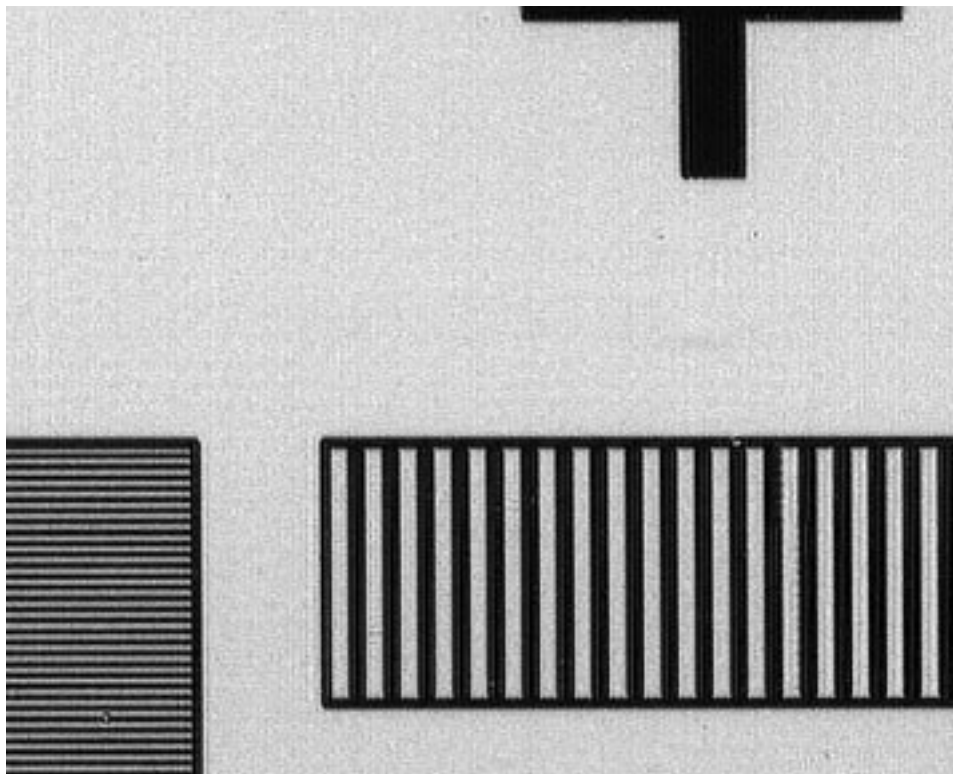


(b)

Fig. 6. (a) High-resolution reconstructed images using standard SRR with a Gaussian blur of standard deviation $\sigma = 1.5$ and (b) the result of SRR with the proposed regularization method (using the same set of images/parameters).



(a)



(b)

Fig. 7. (a) High-resolution reconstructed images using standard SRR with a Gaussian blur of standard deviation $\sigma = 1.8$ and (b) the result of SRR with the proposed regularization method.

IV. CONCLUSIONS

We have proposed methods to improve the accuracy and robustness of POCS-based SRR methods. The following conclusions are noted.

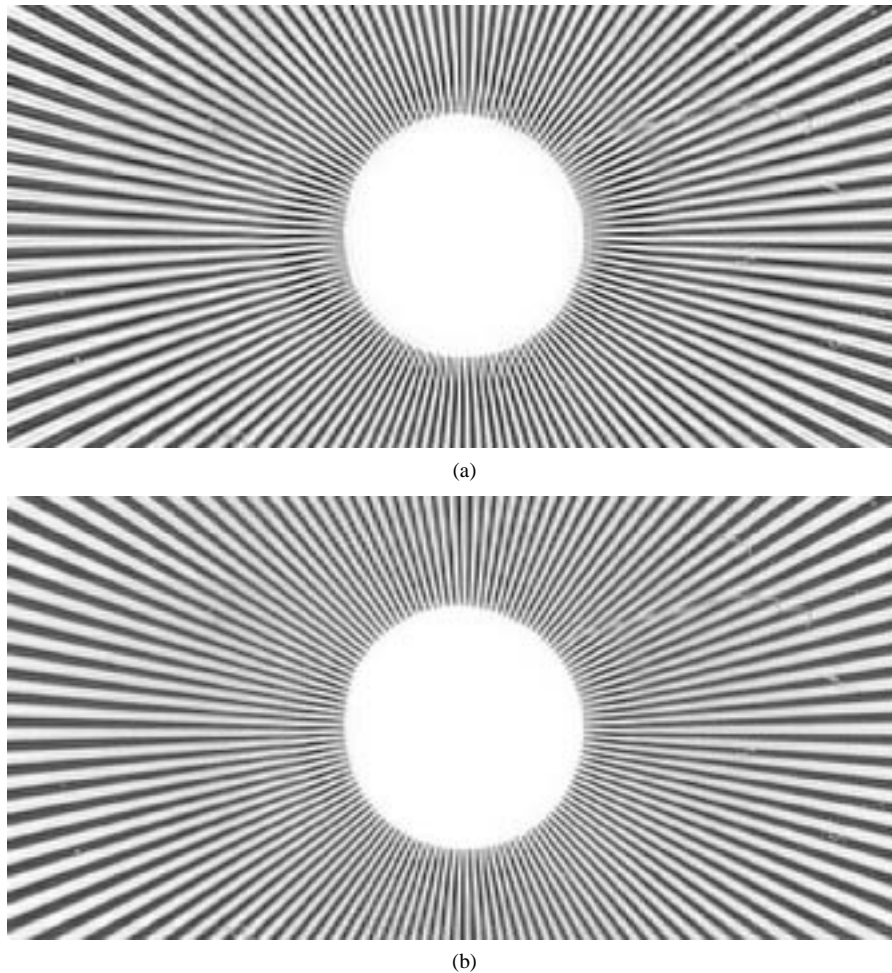


Fig. 8. (a) High-resolution reconstructed images using standard SRR with a Gaussian blur of standard deviation $\sigma = 1.3$ and (b) the result of SRR with the proposed regularization method.

- It is shown that function approximation via higher order interpolants can be encapsulated into POCS-based SRR by convolving the blur function with the interpolant. This incorporation of higher-order interpolants in SRR algorithms significantly improves their accuracy. The proposed changes only affect the blur tables, hence have no effects on the computational cost of SRR algorithms.
- The edge adaptive constraint sets reduce the artifacts, especially when the blur estimates are not correct. Also, additional computational complexity for edge detection is very small.

REFERENCES

- [1] A. J. Patti, M. I. Sezan, and A. M. Tekalp, "Superresolution video reconstruction with arbitrary sampling lattices and nonzero aperture time," *IEEE Trans. Image Processing*, vol. 6, pp. 1064–1076, Aug. 1997.
- [2] M. Elad and A. Feuer, "Restoration of a single superresolution image from several blurred, noisy and undersampled measured images," *IEEE Trans. Image Processing*, vol. 6, pp. 1646–1658, Dec. 1997.
- [3] R. R. Schultz and R. L. Stevenson, "Extraction of high-resolution frames from video sequences," *IEEE Trans. Image Processing*, vol. 5, pp. 996–1011, June 1996.
- [4] R. Y. Tsai and T. S. Huang, "Multiframe image restoration and registration," in *Advances in Computer Vision and Image Processing*, T. S. Huang, Ed. Greenwich, CT: JAI, 1984, ch. 7.
- [5] M. Irani and S. Peleg, "Motion analysis for image enhancement: Resolution, occlusion, and transparency," *J. Vis. Commun. Image Represent.*, vol. 4, pp. 324–335, Dec. 1993.
- [6] P. L. Combettes, "The foundations of set theoretic estimation," *Proc. IEEE*, vol. 81, pp. 182–208, Feb. 1993.
- [7] M. I. Sezan, "An overview of convex projections theory and its applications to image recovery problems," *Ultramicroscopy*, no. 40, pp. 55–67, 1992.
- [8] R. L. Stevenson, B. E. Schmitz, and E. J. Delp, "Discontinuity preserving regularization of inverse visual problems," *IEEE Trans. Syst., Man, Cybern.*, vol. 24, pp. 455–469, Mar. 1994.
- [9] R. R. Schultz and R. L. Stevenson, "A Bayesian approach to image expansion for improved definition," *IEEE Trans. Image Processing*, vol. 3, pp. 233–242, May 1994.
- [10] A. V. Oppenheim and R. W. Schaffer, *Discrete-Time Signal Processing*. Englewood Cliffs, NJ: Prentice-Hall, 1989.
- [11] R. C. Gonzalez and R. E. Woods, *Digital Image Processing*. Reading, MA: Addison-Wesley, 1992.